


ARTICLE

Palladium-catalyzed synthesis of novel pyrido[3,4-*d*]pyridazin-1(2*H*)-ones as promising α -glucosidase, α -amylase and EGFR inhibitors along with molecular docking

Ashish J. Radia¹ | Jaydeep N. Lalpara¹ | Sanjay D. Hadiyal¹ | Mital Kaneria² | Pravin R. Tirgar³ | Gaurang G. Dubal¹ 

¹Department of Chemistry, School of Science, RK University, Rajkot, India

²Department of Bioscience, Saurashtra University, Rajkot, India

³School of Pharmacy, RK University, Rajkot, India

Correspondence

Gaurang G. Dubal, Department of Chemistry, School of Science, RK University, Rajkot 360020, India.
Email: dr.gaurangdubal@gmail.com

Funding information

Saurashtra University

Abstract

A novel route has been established for the synthesis of novel pyrido[3,4-*d*]pyridazin-1(2*H*)-one derivative. Synthesis of intermediate 4-methyl-7-(piperazin-1-yl)pyrido[3,4-*d*]pyridazin-1(2*H*)-one carried out in the presence of Pd(PPh₃)₂Cl₂ catalyst. Ten novel derivatives were synthesized, isolated, and characterized by various spectroscopic techniques. All synthesized molecules were screened for in silico parameters and evaluated for α -glucosidase and α -amylase inhibitory assay. Furthermore, all synthesized molecules were screened for anticancer activity against human lung cell line (A549), human melanoma cell line (A375) and breast cancer (MCF-7) cell lines and their cytotoxic effects were compared. Among the compounds, 8i showed higher inhibition than standard acarbose in the antidiabetic assay. In addition, 8 g exhibited more potency than positive control doxorubicin on lung, breast, and melanoma cancer cell lines. A molecular docking study was carried out on 1RPK and 4HJO as Epidermal growth factor receptor (EGFR) proteins.

1 | INTRODUCTION

Fused heterocyclic compounds are essential moieties due to their biological significance. Numerous fused heterocyclic moieties have been widely utilized in the field of medicinal chemistry for the past few decades. Among them, pyridazine got considerable attraction due to its diverse biological response. The pyridazine-3(2*H*)-one unit was first reported by E. Fischer by the cyclizing phenylhydrazine of levulinic acid, followed by the oxidation by PCl₅.^[1] Many pyridazine derivatives were found to have acetylcholinesterase inhibitor,^[2] anti-inflammatory,^[3] antibacterial,^[4] analgesic,^[5] anticonvulsant,^[6] and antioxidant^[7] activities. Furthermore, some reported pyridazine

compounds are key intermediates in the synthesis of prazidolol, which have vasodilator and beta-blocking properties.^[8] Pyridazine is a heterocyclic family which highly attractive in the field of modern drug discovery. It can gain more consideration due to various pharmacological responses for instance Emorfazone (analgesic, anti-inflammatory),^[9] Azelastine (antiallergic),^[10] vatalanib (oral tyrosine kinase inhibitor),^[11] Lynparza (Anticancer).^[12] Many marketed drugs have pyridazine as core (Figure 1) Moreover, many pesticides contain pyridazine as core such as pyridaben,^[13] Diclomezine,^[14] Flufenpyr.^[15] It also has significant photophysical properties^[16–18] and is used in functional group transformation.^[19, 20]

Recently, we established various protocols for the synthesis of new types of nitrogen and oxygen-containing heterocycles. We also checked for their potency against various diseases which are often observed in society.

Ashish J. Radia and Jaydeep N. Lalpara contributed equally to this work.

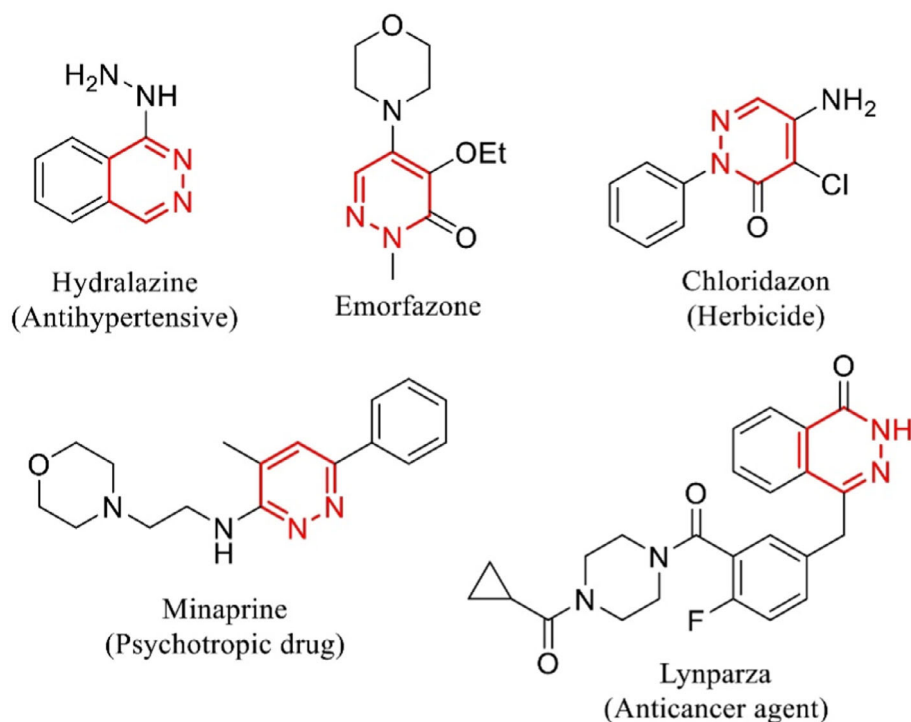


FIGURE 1 Some marketed drugs and active molecules containing pyridazine core

Mainly our contribution to medicinal chemistry is to design and developed antidiabetic, anticancer, antioxidant, and antimicrobial agents.^[21–28]

2 | RESULT AND DISCUSSION

2.1 | Chemistry

Many routes have been established for the synthesis of pyridopyridazinone derivatives. Here in we reported some novel pyrido[3,4-*d*]pyridazin-1(2*H*)-one derivatives by newly synthetic approach. First, Methyl 5-bromo-2-chloroisonicotinate (**1**) react with tributyl(1-ethoxyvinyl) stannane in the presence of Pd(PPh₃)₂Cl₂ catalyst under dioxane solvent for 3 h to get methyl 2-chloro-5-(1-ethoxyvinyl)isonicotinate (**2**). This reaction was optimized by various polar and non-polar solvents as well as varying the amount of catalyst. We found that the reaction proceeds with 1,4-dioxane in good yields. Reaction optimization conditions are mentioned in Table 1. Furthermore, we synthesized an intermediate as 4-methyl-7-(piperazin-1-yl)pyrido[3,4-*d*]pyridazin-1(2*H*)-one (**6**) (yield: 73.4%) outlined in Scheme 1.

Followed by the reaction of 4-methyl-7-(piperazin-1-yl)pyrido[3,4-*d*]pyridazin-1(2*H*)-one hydrochloride (**6**) with different acid halides (**7a–j**) in the presence of triethyl amine (TEA) and tetrahydrofuran (THF) for 2 h at 0°C to rt to get a pure product as **8a–j** outlined in Scheme 2. All synthesized compounds were characterized

by ¹H NMR, ¹³C NMR, mass spectrometry and elemental analysis.

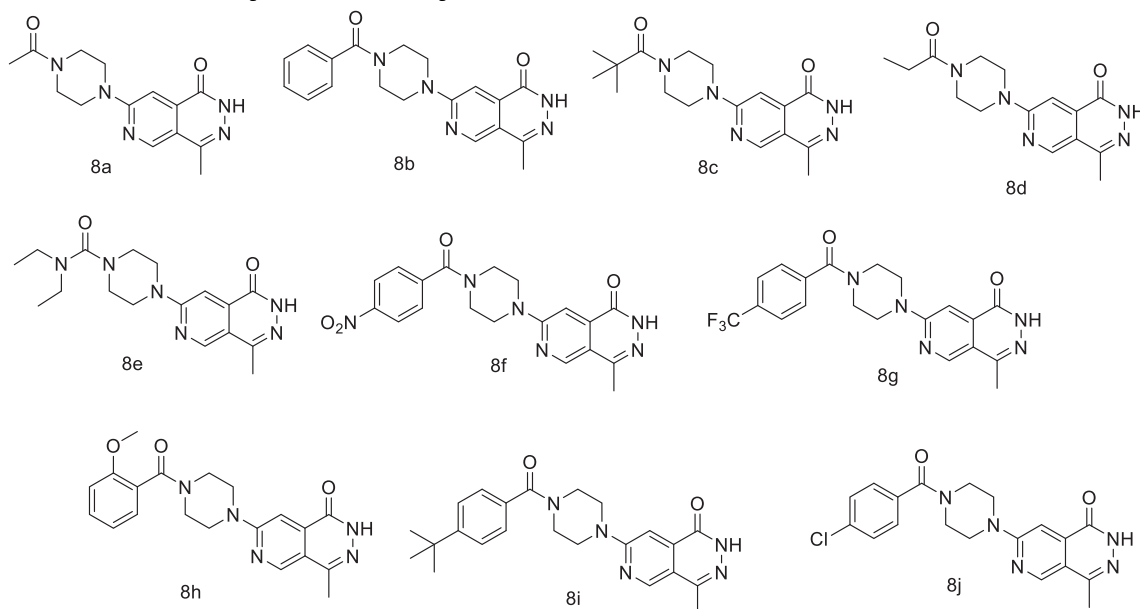
The ¹H NMR spectra of synthesized molecules (**8a–j**) showed broad signals at δ 3.5–3.8 ppm attributed to the aliphatic cyclic ring of piperazine. For pyridazine ring's N-H showed a sharp peak at near 12 δppm. The Methyl group attached to pyridazine ring showed sharp signals near 2 δppm. Aromatic ring protons were observed in the region of the expected chemical shift and showed the estimated integral values for all compounds. Chemical shift and integral values of an aliphatic ring, methyl group and N-H referred to structures of synthesized molecules. ¹³C NMR spectra of **8a–j** revealed that two carbonyl groups are present in each molecule and showed signals at near 165 and 160 ppm. Aliphatic piperazine ring showed a signal in the range of 41–48 ppm. The methyl group of the pyridazine ring showed their signal near 18 ppm.

2.2 | Biological evaluation

2.2.1 | Cytotoxicity

From all synthesized molecules, we identified three lead molecules as **8b**, **8h** and **8j**. we investigated the cytotoxic effects of lead molecules by various methods such as brine shrimp lethality assay and the allium cepa model. Methotrexate was used as a reference drug and all results were compared with it.

TABLE 1 Reaction optimization for compound 2.



Entry	Solvent	Catalyst (mol%) ^a	Temp (°C)	Time (h)	Yield (%) ^b
1	EtOH	Pd(PPh ₃) ₂ Cl ₂ (12%)	Reflux	5 h	38.66
2	MeOH	Pd(PPh ₃) ₂ Cl ₂ (12%)	Reflux	5 h	37.19
3	MeCN	Pd(PPh ₃) ₂ Cl ₂ (12%)	Reflux	4 h	58.71
4	THF	Pd(PPh ₃) ₂ Cl ₂ (12%)	Reflux	4 h	54.45
5	EtOAc	Pd(PPh ₃) ₂ Cl ₂ (12%)	Reflux	5 h	52.29
6	1,4-dioxane	Pd(PPh ₃) ₂ Cl ₂ (12%)	Reflux	4 h	71.67
7	1,4-dioxane	Pd(PPh₃)₂Cl₂ (16%)	Reflux	3 h	76.32
8	1,4-dioxane	Pd(PPh ₃) ₂ Cl ₂ (20%)	Reflux	3 h	75.86

Note: Bold value indicates final optimal condition.

^aCatalyst used in mol (%).

^bIsolated yield.

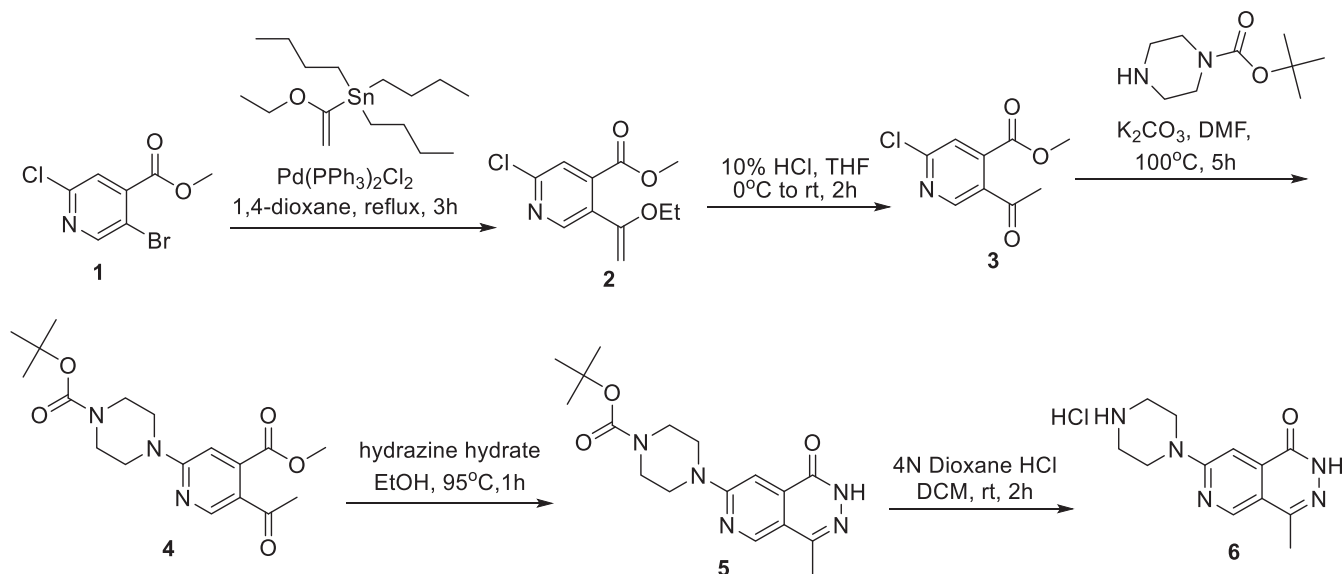
The Brine Shrimp lethality assay has been proven a convenient method for analysis of cytotoxic biological activities. The concentration-dependent death of the nauplius was observed at different time intervals in standard Methotrexate as well as **8b**, **8h** and **8j** treated groups. The highest cytotoxic effect was observed at the concentration of 100 µg/ml in the methotrexate group. **8j** shows maximum cytotoxic action compared to **8b** and **8h**. Mortality of Methotrexate and molecules are mentioned in Table 2.

The decrease in the number of roots and length size is an indicator of inhibition of cell multiplication and so cell division process which directly indicate the screening compounds have action on cell cycle to stop rapidly growing cell. The methotrexate group shows a highly significant reduction in the length and roots as compared to the normal control group suggesting the anticancer effect by inhibiting the cell cycle. The compounds **8b**, **8h** and **8j** show reduce in number of length and roots indicating anticancer activity by acting on the cell cycle (Table 3).

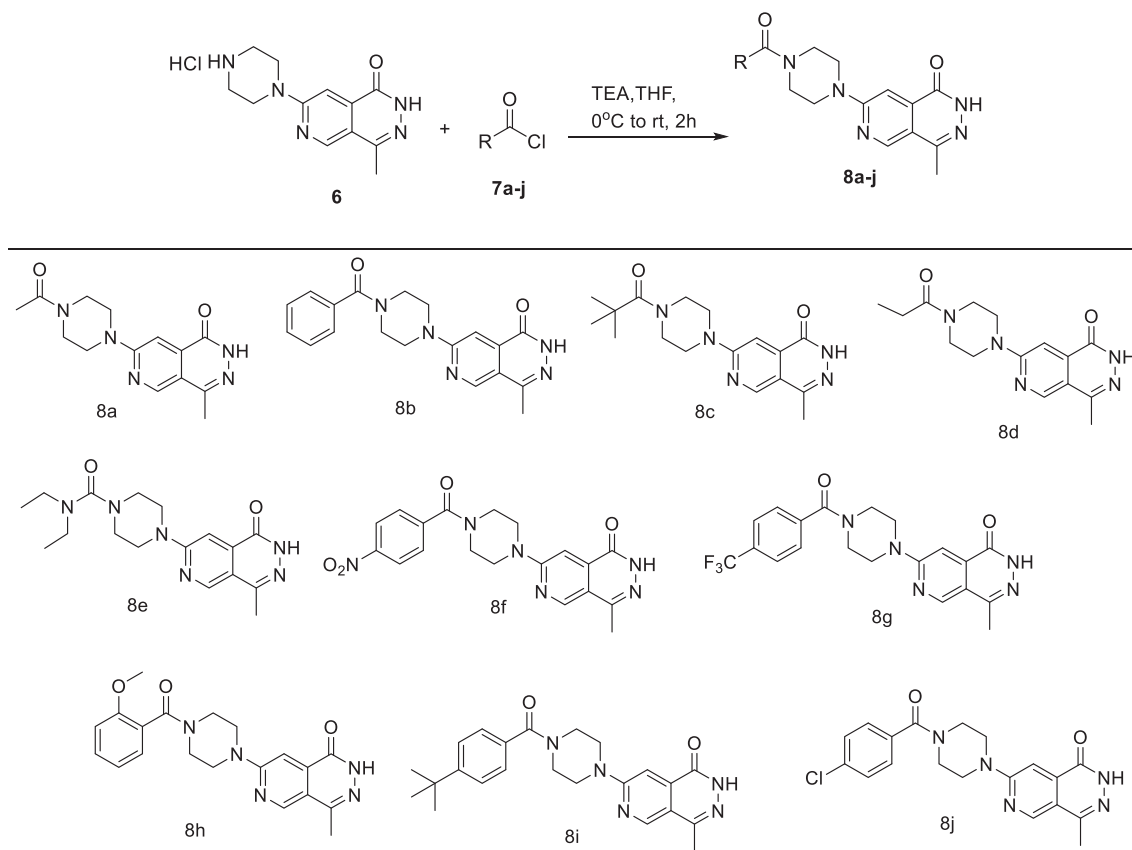
There was concentration-dependent action observed. The potency of **8j** commands shows the highest compared to other and near to methotrexate. To check the significance of data; following statistical tests were performed: ANOVA: to see the variability within all the groups. Tuckey's test: For the same purpose mentioned in the above test. Data were considered statistically significant at $p < 0.05$ and highly significant at $p < 0.01$. Statistical analysis was performed using INSTAT statistical software.

2.2.2 | Anticancer activity

In continuation, the pyrido[3,4-*d*]pyridazin-1(2*H*)-ones (**8a-j**) were screened for in vitro anticancer activity by using MTT assay. The in vitro anticancer activity of **8a-j** was studied on lung (A549), melanoma (A375) and breast (MCF-7) cancer cell lines using doxorubicin as positive



SCHEME 1 Palladium-catalyzed synthesis of 4-methyl-7-(piperazin-1-yl)pyrido[3,4-*d*]pyridazin-1(2*H*)-one hydrochloride



SCHEME 2 Synthesis of pyrido[3,4-*d*]pyridazin-1(2*H*)-one derivatives

control. The obtained results were outlined in Table 4. Results revealed that all synthesized molecules showed a moderate to significant inhibition with IC_{50} values ranging between 1.07 ± 0.06 to 30.48 ± 0.70 μM . Whereas, the standard doxorubicin showed ranging between 1.97 ± 0.80 to 5.89 ± 0.53 μM . Among them, three molecules

8b, **8g** and **8h** showed potent or equal inhibition than standard doxorubicin. Further, these molecules investigated structure activity relationship (SAR) and indicated that compound **8g** having trifluoro substitution exhibits potent anticancer activity on all three cancer cell lines (A549, A375, MCF-7) with IC_{50} 2.08 ± 0.19 , 4.11 ± 0.79 ,

TABLE 2 % Mortality screening of methotrexate and synthesized molecules

Time (h)	% Mortality												
	Control	Methotrexate ($\mu\text{g/ml}$)			8b ($\mu\text{g/ml}$)			8h ($\mu\text{g/ml}$)			8j ($\mu\text{g/ml}$)		
		10	50	100	10	50	100	10	50	100	10	50	100
0	0	0	0	0	0	0	0	0	0	0	0	0	0
1	0	10 ^a	20 ^a	30 ^b	10 ^a	20 ^a	20 ^a	10 ^a	10 ^a	20 ^a	10 ^a	20 ^a	30 ^b
2	0	30 ^b	40 ^b	50 ^b	10 ^a	30 ^b	40 ^b	10 ^a	10 ^a	30 ^b	30 ^b	40 ^b	50 ^b
3	10	40 ^b	50 ^b	70 ^b	20 ^a	40 ^b	60 ^b	30 ^a	30 ^a	40 ^b	50 ^b	50 ^b	60 ^b
6	10	60 ^b	70 ^b	100 ^b	30 ^b	60 ^b	80 ^b	40 ^b	40 ^b	60 ^b	60 ^b	60 ^b	70 ^b
9	10	70 ^b	80 ^b	100 ^b	40 ^b	70 ^b	90 ^b	40 ^b	50 ^b	70 ^b	60 ^b	70 ^b	90 ^b
12	10	80 ^b	100 ^b	100 ^b	50 ^b	80 ^b	100 ^b	50 ^b	60 ^b	80 ^b	80 ^b	90 ^b	100 ^b
24	20	90 ^b	100 ^b	100 ^b	60 ^b	90 ^b	100 ^b	50 ^b	60 ^b	90 ^b	90 ^b	100 ^b	100 ^b

^aIndicate statistical significance compared to normal control group, ($p < 0.05$).

^bIndicate statistical highly significance compared to normal control group, ($p < 0.01$).

TABLE 3 Change is the number of roots treated with methotrexate and synthesized molecules

Group	Concentration ($\mu\text{g/ml}$)	Days					
		1	2	3	4	5	6
Normal concentration	-	4	8	13	26	39	54
Methotrexate	100	1 ^b	2 ^b	3 ^b	4 ^b	6 ^b	7 ^b
	50	2 ^a	4 ^a	6 ^b	7 ^b	8 ^b	10 ^b
	10	3 ^a	4 ^a	7 ^b	10 ^b	13 ^b	14 ^b
8b	100	1 ^b	5 ^a	9 ^a	16 ^a	18 ^b	20 ^b
	50	2 ^a	6 ^a	11 ^a	14 ^a	20 ^a	23 ^b
	10	3 ^a	7 ^a	12 ^a	19 ^a	24 ^a	33
8h	100	1 ^b	6 ^a	10 ^a	18 ^a	24 ^a	29 ^b
	50	2 ^a	7 ^a	13 ^a	19 ^a	26 ^a	32 ^a
	10	4 ^a	9 ^a	14 ^a	21 ^a	33 ^a	39 ^a
8j	100	2 ^a	5 ^a	8 ^a	9 ^b	12 ^b	15 ^b
	50	3 ^a	8 ^a	11 ^a	15 ^a	18 ^b	20 ^b
	10	4 ^a	9 ^a	13 ^a	17 ^a	19 ^b	22 ^b

Note: Length of roots in mm.

^aIndicate statistical significance compared to a normal control group, ($p < 0.05$).

^bIndicate statistical highly significance compared to a normal control group, ($p < 0.01$).

$1.07 \pm 0.06 \mu\text{M}$ respectively. Compounds **8b** (aryl-substituted) and **8h** (2-methoxy aryl-substituted) exhibit the second highest anticancer activity. The halogen-containing analog (**8j**) showed similar activity with nitro and trimethyl analogs. In the electron-donating substitution, the analogs with methyl (**8a**) and ethyl (**8d**) groups on final adducts exhibit less activity than nitro-substituted (**8f**) and trimethyl-substituted (**8i**) product. In conclusion of this study, analogs with donating groups (**8h**) or withdrawing groups (**8b** and **8g**) on pyrido[3,4-*d*]pyridazin-1(2*H*)-ones were found to be the most active compounds in the series.

2.2.3 | In vitro α -glucosidase and α -amylase inhibitory activity

The antidiabetic potentials of Pyrido[3,4-*d*]pyridazin-1(2*H*)-one derivatives (**8a–j**) were evaluated through α -amylase and α -glucosidase inhibition under in vitro conditions. The resulting IC_{50} values of the tested compounds are mentioned in Table 5. Among all synthesized compounds, **8a**, **8i** and **8j** exhibited promising α -amylase and α -glucosidase inhibitory potencies with IC_{50} (α -glucosidase and α -amylase) 11.85 ± 1.03 & 119.81 ± 0.82 , 3.04 ± 0.06 & 29.91 ± 0.44 , 4.29 ± 0.27 and 43.68

Sr No	Compound	A549	A375	MCF-7
1	8a	30.48 ± 0.70	-	-
2	8b	3.19 ± 0.32	5.73 ± 0.29	1.88 ± 0.07
3	8c	18.84 ± 0.52	22.84 ± 0.16	-
4	8d	23.46 ± 0.22	-	-
5	8 e	-	23.18 ± 1.03	17.05 ± 0.94
6	8f	15.67 ± 0.61	18.96 ± 0.04	10.89 ± 0.37
7	8 g	2.08 ± 0.19	4.11 ± 0.79	1.07 ± 0.06
8	8 h	3.30 ± 0.87	5.74 ± 0.09	2.08 ± 0.28
9	8i	16.06 ± 1.35	-	15.81 ± 0.63
10	8j	16.21 ± 0.63	19.50 ± 0.67	-
11	Doxorubicin	2.35 ± 0.41	5.89 ± 0.53	1.97 ± 0.80

TABLE 4 In vitro anticancer activity of synthesized adducts 8a-j in IC₅₀ μM

Note: The results were expressed as the (IC₅₀ μM), values are mean ± SEM and “-” = Not active. DMSO had taken as negative control and given values are subtracted from negative control.

TABLE 5 In vitro antidiabetic screening of synthesized compounds (8a-j)

Sr. No.	Compound	Antidiabetic (IC ₅₀ μM)	
		α-Glucosidase	α-Amylase
1	8a	11.85 ± 1.03	119.81 ± 0.82
2	8b	>250	>250
3	8c	>250	>250
4	8d	98.74 ± 0.69	>250
5	8 e	110.19 ± 1.12	>250
6	8f	>250	>250
7	8 g	>250	>250
8	8 h	>250	>250
9	8i	3.04 ± 0.06	29.91 ± 0.44
10	8j	4.29 ± 0.27	43.68 ± 0.97
11	Acarbose	3.93 ± 0.18	36.11 ± 0.05

Note: The results were expressed as the (IC₅₀ μM), values are mean ± SEM.

± 0.97 μM. The SAR analysis showed that the nature of substituents on aryl position of pyrido[3,4-*d*]pyridazin-1 (2*H*)-ones significantly affected their inhibitory potency. Compound **8i** with *para*-trimethyl substitution showed the highest inhibition of α-glucosidase and α-amylase in the series with IC₅₀ 3.04 ± 0.06, 29.91 ± 0.44 μM, respectively, and was 1.3-fold more than the reference drug (IC₅₀ = 3.93 ± 0.18 μM). This improved biological response might be because of the electron-donating nature of trimethyl substituent. In contrast, more than 100-fold inferior activity of *para*-fluoro-substituted compound **8g** as compared to compounds **8i** and **8j**.

Interestingly, the good α-glucosidase and α-amylase inhibition potency were observed with compound **8j**

with IC₅₀ value of 4.29 ± 0.27, 43.68 ± 0.97 μM. The second highest inhibition was observed with compound **8j** due to the *para*-chloro substituent. In contrast, compounds **8c**, **8d** which having alkyl substitution showed very less inhibition. On the other hand, when phenyl and nitrogen substitutions on synthesized molecules (**8b** and **8e**) showed lower inhibition potential (IC₅₀ = >250 μM).

2.3 | Molecular docking

2.3.1 | Docking on 1RPK receptor

The field of molecular docking has emerged during the last few decades and now is becoming an integral aspect in drug discovery and development area. Binding energies are the most widely used mode of measuring binding affinity of the screened compounds carried out by Argus lab in Table 6. The virtual screening revealed that all the inhibitors (**8a-j**) except a few shown strong affinities with almost similar docking score (Table 6). Moreover, **8a**, **8i** and **8j** possess remarkable activity with high specificity and selectivity towards the receptor. Figure 2 exemplifies the diagrammatical representation of molecular docking analysis of selected ligand (**8i**) with protein 1RPK by Argus lab and visualization of docked protein by Discovery Studio. Molecular docking analysis of Ligand (**8i**) with protein 1RPK by ArgusLab showed interaction with amino acids TYR52, ARG178, ASP180, ARG183, GLU205, TRP207, ASN209, HIS290, ASP291 & MET298 by forming different types of bonds with various bond length represented using Argus Lab (Figure 2A) and Discovery Studio software in 3D (Figure 2B) and in 2D (Figure 2C). Therefore, molecular docking study

TABLE 6 Docking score of screened compounds and Acarbose against 1RPK receptor

Sr. No.	Compound	Docking score (ΔG kcal/mol)	No. of pose
1	8a	-5.37	8
2	8b	-5.1	3
3	8c	-4.89	54
4	8d	-5.05	2
5	8 e	-5.03	13
6	8f	-4.76	2
7	8 g	-3.27	1
8	8 h	-4.98	3
9	8i	-6.76	3
10	8j	-5.88	4
11	Acarbose	-5.32	7

exhibited that many compounds have significant interactions within the active site residues of α -amylase receptor which might be the cause of remarkable α -amylase inhibition activity.

2.3.2 | Docking on EGFR receptor

To understand the binding interaction of most active compounds, molecular docking studies were performed. Protein EGFR is found on the surface of some normal cells and is involved in cell division and cell growth. Blocking of EGFR may control the growth of cancer cells and hence EGFR inhibitors are used in cancer treatment. Recent studies have shown that tyrosine kinase inhibitors (TKIs) involving mutations to the EGFR, are used for initial lung cancer therapy.^[29] All tested cancer cell lines (melanoma, lung, breast) were inhibited better compared with reference drug for some compounds. Thus, we have chosen protein EGFR for molecular docking studies. Result revealed that, the compound 8g binds strongly to EGFR receptor with lowest binding energy -9.8 kcal/mol. On other hand, binding energy of 8b and 8h are -9.4 and -9.2 kcal/mol respectively (Table 7). The docking results were in great concurrence with experimental IC_{50} values displayed in Table 4.

Figure 3 shows the best conformation pose of compound 8g forming a cluster with EGFR receptor. Docking result revealed that the EGFR protein having amino acids Lys855, Ile854, Trp856, Lys851, Pro853, Phe699, Asp813, Ala835, and Leu834 are the most active sites and responsible for interaction with 8g. In this cluster, strong conventional hydrogen bonds are observed with Lys855 and Ile854 with compound 8g with a distance of 2.08 and 2.55 Å respectively (Table 8). Additionally, some non-hydrogen bonding interactions were observed with Trp856, Lys851, Pro853, Phe699, Asp813, Ala835, and Leu834 amino acids. In conclusion of SAR, the

experimental results effectively correlated with the molecular docking analysis.

3 | CONCLUSIONS

In conclusion, we developed a new protocol for the synthesis of novel series of pyrido[3,4-*d*]pyridazin-1(2*H*)-ones. All synthesized molecules were studied for molecular docking studies. Furthermore, all molecules were evaluated for α -glucosidase and α -amylase inhibitory assay. Results of the antidiabetic study revealed that compound 8i exhibited higher potential than standard drug acarbose. In addition, a molecular docking study on 1RPK receptor also supports this study with the lowest binding score (-6.76 kcal/mol). Additionally, all molecules were checked for their anticancer potential on lung (A549), melanoma (A375) and breast cancer (MCF-7) cell lines. The result of in vitro anticancer evaluation indicates that the compound 8g has more potency than positive control doxorubicin. On other hand, compounds 8b and 8h have shown good potency on all three cancer cell lines. A molecular docking study also indicates that the promising compounds 8b, 8g and 8h have the lowest binding energies with EGFR (4HJO) receptor with -9.4 , -9.8 , -9.2 kcal/mol respectively. The result reveals that the compounds serve as promising leads to develop a new class of antidiabetic and anticancer drugs.

4 | EXPERIMENTAL

4.1 | Chemistry

4.1.1 | Materials and methods

All chemicals were purchased from different supplier like sigma Aldrich, combi-block, enamine, etc., all

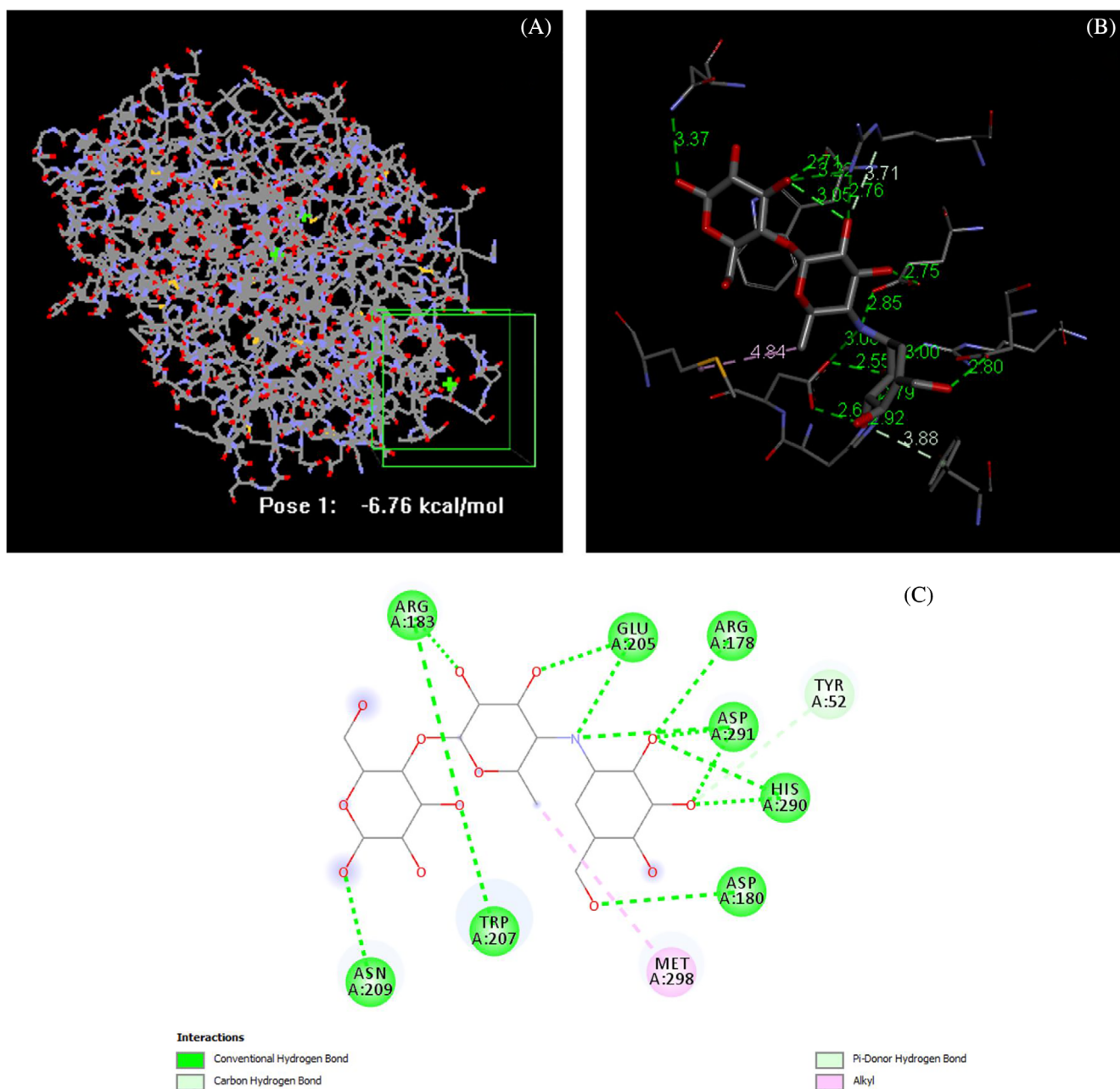


FIGURE 2 Molecular docking analysis on binding site interaction of 8i with receptor 1RPK (A) binding position of ligand by using ArgusLab, (B) 3D visualization of ligand and amino acid residues of protein by using discovery studio, (C) 2D representation of ligand and protein interaction visualized by discovery studio.

purchased chemicals were used without further purification, Reactions were monitored by thin layer chromatography (TLC) on silica gel-G plates (G60 F254 (Merck)) of 0.5 mm thickness, visualizing with ultraviolet light (254 and 365 nm), or with iodine vapor or aq. KMnO_4 . Melting points were determined using a Buchi B-540 capillary apparatus. NMR spectra were recorded on a Bruker Advance 400 MHz spectrometer (400 MHz for ^1H NMR and 101 MHz for ^{13}C NMR) respectively in solvents like DMSO and CDCl_3 and

chemical shifts are referenced to the solvent residual signals with respect to tetramethylsilane. Elemental analysis was carried out on Euro EA 3000 elemental analyzer and the results agree with the structures assigned. The control of reaction temperature was monitored by ruby thermometer. Mass spectra were recorded on a Shimadzu GC-MS-QP-2010 mass spectrometer in EI (70 eV) model using direct inlet probe technique and m/z is reported in atomic units per elementary charge.

TABLE 7 Docking score of compounds (8a–j) and doxorubicin against EGFR receptor

Sr No	Compound	Docking score (ΔG kcal/mol)
1	8a	-7.7
2	8b	-9.4
3	8c	-8.5
4	8d	-7.8
5	8e	-8.4
6	8f	-8.6
7	8g	-9.8
8	8h	-9.2
9	8i	-8.4
10	8j	-8.4
11	Doxorubicin	-9.6

4.1.2 | General procedure for synthesis of pyrido[3,4-*d*]pyridazin-1(2*H*)-ones (8a–j)

To a stir solution of 4-methyl-7-(piperazin-1-yl)pyrido[3,4-*d*]pyridazin-1(2*H*)-one hydrochloride (0.35 mmol) in THF (2 ml) TEA (1.06 mmol) was added and reaction mixture was stirred at rt for 15 min then acetyl chloride (0.45 mmol) was added at 0°C, then reaction mixture was stirred at rt for 2 h. Progress of reaction was monitored by TLC. After completion of reaction, reaction mixture was poured into water (10 ml), solid material was precipitated out which was filtered out and washed with water (10 ml) and diethyl ether (10 ml), dried under vacuum to get pure pyrido[3,4-*d*]pyridazin-1(2*H*)-ones (7a–j) (60–72%) as a solid materials.

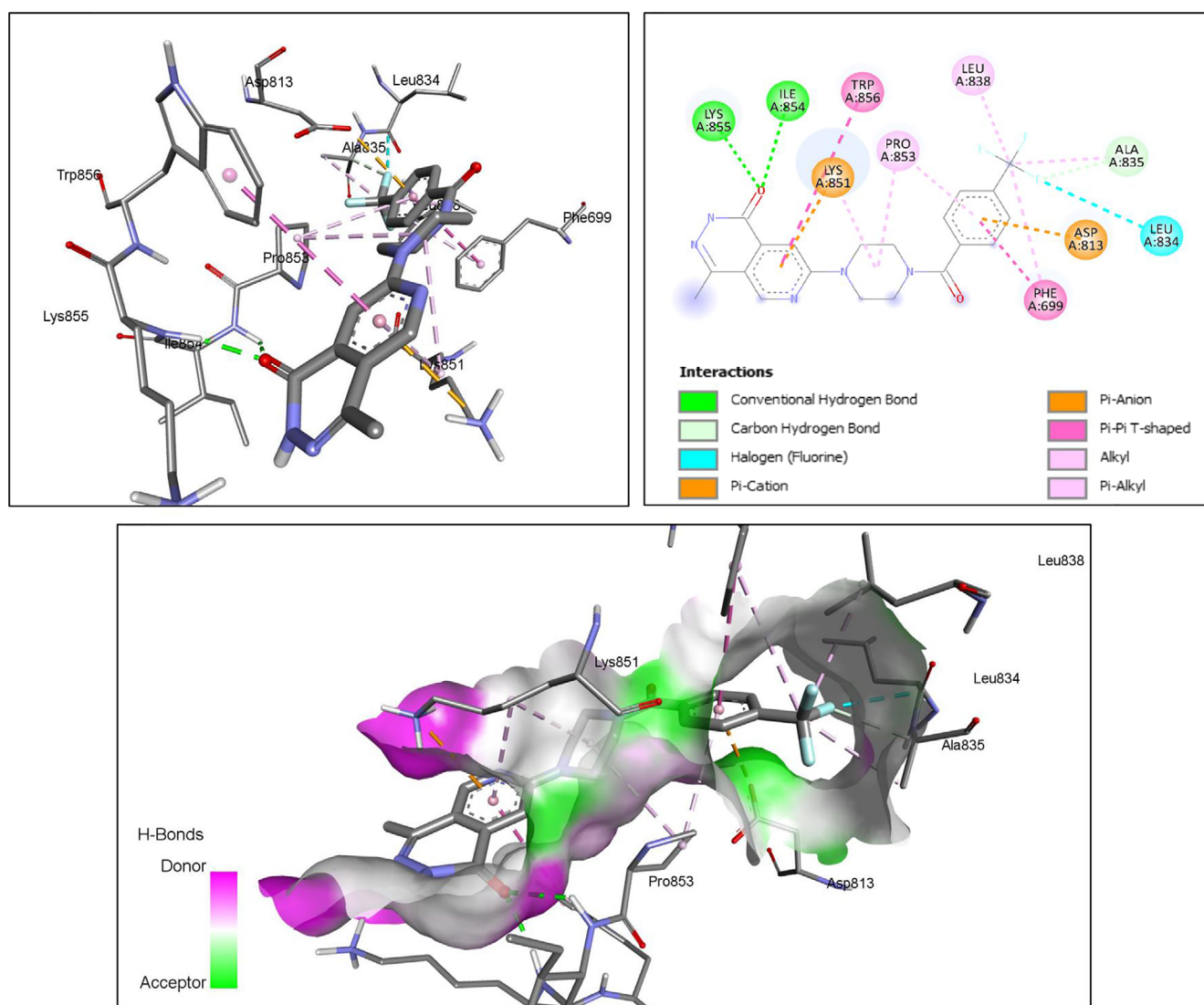


FIGURE 3 Binding poses and interactions of compound 8g to the binding sites of EGFR receptor

TABLE 8 Binding energy, hydrogen bond and residues involved in H-bond of compounds 8b, 8g and 8h

Sr No	Compound	Binding energy (kcal/mol)	Number of hydrogen bonds	Residues involved in H-bonding
1	8b	-9.4	1	Lys851
2	8g	-9.8	2	Lys855, Ile854
3	8h	-9.2	1	Lys851

4.1.3 | Spectral data for products

7-(4-acetylpiperazin-1-yl)-4-methylpyrido[3,4-d]pyridazin-1(2H)-one (8a) off white solid, yield—64.61%. Mp: 174–176°C. ¹H NMR (400 MHz, DMSO-*d*₆): δ = 12.25 (s, 1H, NH), 8.89 (s, 1H, H-Ar), 7.23 (s, 1H, H-Ar), 3.72 (m, 4H, CH₂), 3.58 (m, 4H, CH₂), 2.48 (d, *J* = 14.8 Hz, 3H, CH₃), 2.05 (s, 3H, CH₃). ¹³C NMR (101 MHz, DMSO-*d*₆): δ = 169.00, 159.54, 159.20, 149.41, 143.16, 135.27, 116.00, 98.42, 46.21, 45.50, 44.81, 44.55, 21.75, 18.14. Mass *m/z*: 350.63. Elemental analysis: C₁₉H₁₉N₅O₂, calculated: C, 65.32; H, 5.48; N, 20.04; Found: C, 65.22; H, 5.51; N, 20.13.

7-(4-benzoylpiperazin-1-yl)-4-methylpyrido[3,4-d]pyridazin-1(2H)-one (8b) grayish white solid, yield—61.72%. Mp: 174–176°C. ¹H NMR (400 MHz, DMSO-*d*₆): δ = 12.26 (s, 1H, NH), 8.89 (s, 1H, H-Ar), 7.47 (d, *J* = 1.6 Hz, 5H, H-Ar), 7.24 (s, 1H, H-Ar), 3.81–3.75 (m, 6H, CH₂), 3.49 (m, 2H, CH₂), 2.46 (s, 3H, CH₃). ¹³C NMR (101 MHz, DMSO-*d*₆): δ = 169.71, 159.47, 159.16, 149.43, 143.11, 136.24, 135.24, 130.15, 128.94, 127.54, 116.05, 98.49, 47.05, 44.55, 41.83, 18.14. Mass *m/z*: 350.63, Elemental analysis: C₁₉H₁₉N₅O₂, calculated: C, 65.32; H, 5.48; N, 20.04; Found: C, 65.30; H, 5.43; N, 20.07.

4-methyl-7-(4-pivaloylpiperazin-1-yl)pyrido[3,4-d]pyridazin-1(2H)-one (8c) white solid, yield—63.76%. Mp: 182–184°C. ¹H NMR (400 MHz, DMSO-*d*₆): δ = 12.25 (s, 1H, NH), 8.89 (s, 1H, H-Ar), 7.22 (s, 1H, H-Ar), 3.69 (m, 8H, CH₂), 2.48 (s, 3H, CH₃), 1.23 (s, 9H, CH₃). ¹³C NMR (101 MHz, DMSO-*d*₆): δ = 175.75, 159.63, 159.17, 149.36, 143.12, 135.21, 116.04, 98.34, 44.89, 44.60, 38.58, 28.52, 27.48, 18.14. Mass *m/z*: 330.55, Elemental analysis: C₁₇H₂₃N₅O₂, calculated: C, 61.99; H, 7.04; N, 21.26; Found: C, 61.96; H, 7.05; N, 21.33.

4-methyl-7-(4-propionylpiperazin-1-yl)pyrido[3,4-d]pyridazin-1(2H)-one (8d) light pink solid, yield—64.61%. Mp: 170–172°C. ¹H NMR (400 MHz, DMSO-*d*₆): δ = 12.31 (s, 1H, NH), 8.91 (s, 1H, H-Ar), 7.34 (s, 1H, H-Ar), 3.92 (m, 4H, CH₂), 3.18–3.17 (m, 4H, CH₂), 3.05 (q, *J* = 14.4 Hz, 7.2 Hz, 2H, CH₂), 2.47 (s, 3H, CH₃), 1.18 (t,

J = 7.2 Hz, 3H, CH₃). ¹³C NMR (101 MHz, DMSO-*d*₆): δ = 159.11, 149.33, 143.13, 135.37, 116.57, 99.06, 45.82, 42.70, 41.87, 18.20, 8.92. Mass *m/z*: 302.49. Elemental analysis: C₁₅H₁₉N₅O₂, calculated: C, 59.79; H, 6.36; N, 23.24; Found: C, 59.81; H, 6.31; N, 23.25.

N,N-diethyl-4-(4-methyl-1-oxo-1,2-dihydropyrido[3,4-d]pyridazin-7-yl)piperazine-1-carboxamide (**8e**) pale yellow solid, yield—65.33%. Mp: 184–186°C. ¹H NMR (400 MHz, DMSO-*d*₆): δ = 12.24 (s, 1H, NH), 8.88 (s, 1H, H-Ar), 7.22 (s, 1H, H-Ar), 3.71 (m, 4H, CH₂), 3.22 (m, 4H, CH₂), 3.16 (q, *J* = 14.0 Hz, 6.8 Hz, 4H, CH₂), 2.45 (s, 3H, CH₃), 1.06 (t, *J* = 6.8 Hz, 6H, CH₃). ¹³C NMR (101 MHz, DMSO-*d*₆): δ = 163.86, 159.62, 159.16, 149.24, 143.05, 135.15, 115.92, 98.27, 46.74, 44.55, 41.70, 18.11, 13.51. Mass *m/z*: 345.66. Elemental analysis: C₁₇H₂₄N₆O₂, calculated: C, 59.28; H, 7.02; N, 24.40; Found: C, 59.33; H, 7.09; N, 24.30.

4-methyl-7-(4-(4-nitrobenzoyl)piperazin-1-yl)pyrido[3,4-d]pyridazin-1(2H)-one (8f) yellow solid, yield—61.81%. Mp: 188–190°C. ¹H NMR (400 MHz, DMSO-*d*₆): δ = 12.26 (s, 1H, NH), 8.89 (s, 1H, H-Ar), 8.31 (d, *J* = 8.40 Hz, 2H, H-Ar), 7.74 (d, *J* = 8.00 Hz, 2H, H-Ar), 7.25 (s, 1H, H-Ar), 3.86–3.73 (m, 6H, CH₂), 3.43 (m, 2H, CH₂), 2.46 (s, 3H, CH₃). ¹³C NMR (101 MHz, DMSO-*d*₆): δ = 167.82, 159.47, 159.17, 149.43, 148.37, 143.15, 142.56, 135.29, 128.92, 124.29, 116.13, 98.56, 46.85, 44.89, 44.32, 41.79, 18.15. Mass *m/z*: 395.80. Elemental analysis: C₁₉H₁₈N₆O₄, calculated: C, 57.86; H, 4.60; N, 21.31; Found: C, 57.89; H, 4.54; N, 21.32.

4-methyl-7-(4-(4-(trifluoromethyl)benzoyl)piperazin-1-yl)pyrido[3,4-d]pyridazin-1(2H)-one (8g) white solid, yield—71.88%. Mp: 170–172°C. ¹H NMR (400 MHz, DMSO-*d*₆): δ = 12.26 (s, 1H, NH), 8.90 (s, 1H, H-Ar), 7.85 (d, *J* = 7.6 Hz, 2H, H-Ar), 7.69 (d, *J* = 7.6 Hz, 2H, H-Ar), 7.25 (s, 1H, H-Ar), 3.85–3.73 (m, 6H, CH₂), 3.45 (m, 2H, CH₂), 2.46 (s, 3H, CH₃). ¹³C NMR (101 MHz, DMSO-*d*₆): δ = 168.36, 159.50, 159.18, 149.44, 143.16, 140.38, 135.29, 128.38, 126.01, 125.79, 116.12, 98.54, 46.90, 44.95, 44.36, 41.83, 18.15. Mass *m/z*: 418.25. Elemental Analysis: C₂₀H₁₈F₃N₅O₂, calculated: C, 57.55; H, 4.35; N, 16.78; Found: C, 57.51; H, 4.34; N, 16.80.

7-(4-(2-methoxybenzoyl)piperazin-1-yl)-4-methylpyrido[3,4-d]pyridazin-1(2H)-one (8h) white solid, yield—71.88%. Mp: 170–172°C. ¹H NMR (400 MHz, DMSO-*d*₆): δ = 12.25 (s, 1H, NH), 8.88 (s, 1H, H-Ar), 7.42 (t, *J* = 7.2 Hz, 1H, H-Ar), 7.23 (d, *J* = 8.8 Hz, 2H, H-Ar), 7.10 (d, *J* = 8.4 Hz, 1H, H-Ar), 7.01 (t, *J* = 7.6 Hz, 1H, H-Ar), 3.80 (s, 3H, CH₃), 3.75–3.67 (m, 6H, CH₂), 3.26–3.26 (m, 2H, CH₂), 2.46 (s, 3H, CH₃). ¹³C NMR (101 MHz, DMSO-*d*₆): δ = 167.12, 159.51, 159.17, 155.43, 149.38, 143.13, 135.27, 131.00, 128.36, 125.90, 121.17, 116.06, 111.90, 98.54, 55.96, 46.18, 45.15, 44.53, 41.29, 18.14. Mass *m/z*: 380.75. Elemental Analysis: C₂₀H₂₁N₅O₃,

calculated: C, 63.31; H, 5.58; N, 18.46; Found: C, 63.40; H, 5.38; N, 18.44.

7-(4-(4-(*tert*-butyl)benzoyl)piperazin-1-yl)-4-methylpyridido[3,4-*d*]pyridazin-1(2*H*)-one (**8i**) off white solid, yield—70.76%. Mp: 174–176°C. ¹H NMR (400 MHz, DMSO-*d*₆): δ = 12.25 (s, 1H, NH), 8.89 (s, 1H, H-Ar), 7.48 (t, *J* = 8.0 Hz, 2H, H-Ar), 7.39 (d, *J* = 8.0 Hz, 2H, H-Ar), 7.24 (s, 1H, H-Ar), 3.75 (m, 6H, CH₂), 3.53 (m, 2H, CH₂), 2.46 (s, 3H, CH₃), 1.30 (s, 9H, CH₃). ¹³C NMR (101 MHz, DMSO-*d*₆): δ = 169.79, 159.46, 159.16, 152.81, 149.31, 143.09, 135.22, 133.32, 127.55, 125.65, 116.03, 98.45, 47.08, 44.73, 41.92, 35.01, 31.46, 18.13. Mass *m/z*: 406.20. Elemental Analysis: C₂₃H₂₇N₅O₂, calculated: C, 68.13; H, 6.71; N, 17.27; Found: C, 68.33; H, 6.11; N, 17.22.

7-(4-(4-chlorobenzoyl)piperazin-1-yl)-4-methylpyridido[3,4-*d*]pyridazin-1(2*H*)-one (**8j**) gray solid, yield—51.36%. Mp: 186–188°C. ¹H NMR (400 MHz, DMSO-*d*₆): δ = 12.26 (s, 1H, NH), 8.89 (s, 1H, H-Ar), 7.54 (d, *J* = 8.40 Hz, 2H, H-Ar), 7.49 (d, *J* = 8.40 Hz, 2H, H-Ar), 7.24 (s, 1H, H-Ar), 3.82–3.73 (m, 6H, CH₂), 3.47 (m, 2H, CH₂), 2.46 (s, 3H, CH₃). ¹³C NMR (101 MHz, DMSO-*d*₆): δ = 168.67, 159.46, 159.16, 149.36, 143.11, 135.25, 135.00, 134.84, 131.58, 129.58, 129.04, 116.06, 98.49, 47.02, 44.89, 41.88, 18.13. Mass *m/z*: 384.72. Elemental Analysis: C₁₉H₁₈ClN₅O₂, calculated: C, 59.45; H, 4.73; N, 18.25; Found: C, 59.46; H, 4.77; N, 18.20.

4.2 | Biological evaluation

4.2.1 | α-Glucosidase inhibitory activity

The α-glucosidase inhibitory activity of the synthesized compounds was measured according to the previously established procedure.^[30] For each 50 μl of synthesized compound or standard acarbose, liquified in DMSO solvent to afford different concentrations (15, 30, 60, 120, and 240 μg/ml), mixed with a 100 μl of 1.0 ml of α-glucosidase and phosphate buffer (100 mM, pH 6.8), which was incubated in a 96 well plate at 37°C for 20 min. Afterward, 50 μl of 5 mM of p-nitrophenyl-α-D-glucopyranoside (p-NPG) solution was added to the reaction mixture and was further incubated at 37°C. After 30 min, the absorbance was measured at 405 nm and the results are expressed as a percentage of the control sample without inhibitors by the formula:

$$\%inhibition = \left[\frac{\text{absorbance of blank} - \text{absorbance of compound}}{\text{absorbance of blank}} \right] \times 100$$

4.2.2 | α-Amylase inhibitory activity

The α-amylase inhibitory activity was carried out by previously reported method.^[31] In which 250 μl of each synthesized compound (or) acarbose, was dissolved in DMSO to get different concentrations fractions (15, 30, 60, 120 and 240 μg/ml), and was mixed with 500 μl of malt amylase (2 U/ml) in phosphate buffer (100 mM, pH 6.8). Samples were incubated for 10 min at 37°C. Thereafter, 50 μl of 1% starch was dissolving in the same buffer and it was added to the reaction mixture. These samples were incubated at 37°C for a further 30 min. Afterward, dinitrosalicylate (DNS) reagent (1 ml) was mixed into these samples and was further boiled for 10 min. The absorbance was measured at 540 nm and the results were expressed as a percentage of the control by the following formula:

$$\%inhibition = \left[\frac{\text{absorbance of blank} - \text{absorbance of compound}}{\text{absorbance of blank}} \right] \times 100$$

4.2.3 | Anticancer activity (MTT assay)

The cytotoxic activity of the compounds was determined using MTT assay.^[32] 1 × 10⁴ cells/well were seeded in 200 ml DMEM, supplemented with 10% FBS in each well of 96 well microculture plates and incubated for 24 h at 37°C in a CO₂ incubator. Compounds, diluted to the desired concentrations in culture medium, were added to the wells with respective vehicle control. After 48 h of incubation, 10 ml MTT (3-(4,5-dimethylthiazol-2-yl)-2,5-diphenyl tetrazolium bromide) (5 mg/ml) was added to each well and the plates were further incubated for 4 h. Then the supernatant from each well was carefully removed, formazan crystals were dissolved in 100 ml of DMSO and absorbance at 540 nm wavelength was recorded.

4.2.4 | Brine shrimp lethality assay

The Brine Shrimp Lethality Assay is applied as an alternative bioassay method for evaluation of cytotoxicity potential because Brine Shrimp has the ability to rapid growing like a cancer cell in the human body.^[33] We aimed to assess the bioactivity of organic compounds to find new substances with potential pharmaceutical applications. Brine shrimp were ordered from the Amazon online platform and available in capsule form which was

filled with thousands of dried cysts. Dried cysts were performed as indicated above, and then incubated (1 g cyst per lit seawater solution) in a hatcher at 28–30 °C with the appropriate aeration, under a continuous light regime. Approximately after 12 h hatching the phototropic nauplii were collected with a pipette from the lighter side and concentrated in a small vial. Ten brine shrimp were transferred using an adequate pipette. Each test considered exposing groups of 10 *Artemia* aged after 12 h to different concentration and % of deaths were calculated. Larvae were considered dead if they did not exhibit any internal or external movement during the observation. The larvae should not receive food. To ensure that the mortality observed in the bioassay could be attributed to the bioactive compounds and not to starvation. We should compare the dead larvae in each treatment to the control. In the case of hatched brine shrimp nauplii can survive for up to 48 h without food they feed on their yolk sac. Where control deaths were detected, calculated percentage of mortality.

$$\%M = \frac{\text{Percentage of survival in the control} - \text{Percentage of survival in the treatment}}{\text{Percentage of survival in the control}} \times 100$$

4.2.5 | *Allium cepa* model

The *Allium cepa* (onion) root model was used to evaluate the cytotoxic potential of compounds. Onion bulbs (*Allium cepa* L.) were kept at different drug concentrations (10, 50, 100 µg/ml Standard drug methotrexate) and test compounds AR2, AR8 and AR10 (10, 50, 100 µg/ml) containing flask. The root number and root length in mm were measured at a 1-to-6-day interval to screen cytotoxic potential and compared the screening compounds with normal control and standard control methotrexate group.

4.3 | Molecular docking

4.3.1 | Docking on 1RPK receptor

Protein target was downloaded from the database, Protein Data Bank, α-amylase (1RPK)^[34] selected for the present study as protein target. For the ligand preparations, translated using the “Open babel” Translator Molecular Mechanics (MM) method, UFF was used for refining initial geometries, in the ArgusLab Software. The active site was defined from the coordinates in the original PDB file. Residues that lie within 5 Å unit area of ligand that interact with it through their side chain were identified and were considered as active site residues. The docking between receptor and ligand was performed using a

spacing of 0.4 Å between the grid points was used. The binding site box size was set to (15 × 15 × 15 Å) encompass the entire active site. Molecular docking was implemented on 1RPK receptor against ligands using Argus Lab 4.0.1 to find the reasonable binding geometries and to explore the protein–ligand interactions. Docking of the protein–ligand complex was mainly targeted only on the predicted active site. Docking simulations were performed by selecting Argus Dock as the docking engine and their relative stabilities were evaluated using molecular dynamics, and their binding affinities, using free energy simulation, pose, and time. Single trajectory method was used for the binding energy calculation. The selected residues of the receptor were defined to be a part of the binding site and ligand–protein interaction visualized by Biovia Discovery studio.

4.3.2 | Docking on EGFR receptor

The anticancer potency of all the compounds were further screened for molecular docking study to explore the approaching of drug candidates towards the protein and binding pattern against EGFR receptor (PDB ID: 4hjo)^[35] obtained from RCSB Protein data bank. The 2D structures of ligands were drawn in Chem Bio Draw Ultra 14.0 and 3D structures were created by using ChemBio3D Ultra 14.0. For the final preparation of ligand preparations, translated using the “Open babel” Translator Molecular Mechanics (MM) method. The process of making of protein receptor by eliminating the water molecule and addition of polar hydrogen followed by Kollman charge by using Auto dock vina software. The active site was defined from the coordinates in the original PDB file. Auto dock vina (<http://vina.scripps.edu>) was used for the molecular docking. In the docking process, the rigid protein receptor EGFR and compounds 8a-j were involved and in the preliminary step. The distance between donor and acceptor atoms that form a hydrogen bond was fixed as 5.0 Å. For further studies in ADT, initially, the PDB structures were converted in PDBQT format, and grid box with dimensions 56 × 54 × 78 Å created around the EGFR protein receptor assigned with the assistance of Auto Dock Tools and spacing (Angstrom): 0.537 Å. The output results were used to analyze Discovery studio 4.1.0. Software. This explores the clear view of docking studies of 8a-j inhibitors including binding energies of receptor-ligand complex.

ACKNOWLEDGMENTS

The authors are grateful to the RK University and Saunashra University for providing lab facility and CDRI-Lucknow for providing spectral data.

FUNDING INFORMATION

This research did not receive any specific grant from funding agencies in the public, commercial, or not-for-profit sectors.

CONFLICT OF INTEREST

The authors report no conflict of interest.

DATA AVAILABILITY STATEMENT

The data that supports the findings of this study are available in the supplementary material of this article.

ORCID

Gaurang. G. Dubal  <https://orcid.org/0000-0002-0055-5407>

REFERENCES

- [1] P. G. Sergeev, V. N. Khrustalev, V. G. Nenajdenko, *Eur. J. Org. Chem.* **2020**, 38, 6085.
- [2] P. Taslimi, F. Turkan, A. Cetin, H. Burhan, M. Karaman, I. Bildirici, I. Gulcin, F. Sen, *Bioorg. Chem.* **2019**, 92, 103213.
- [3] E. M. Ahmed, M. S. A. Hassan, A. A. El-Malah, A. E. Kassab, *Bioorg. Chem.* **2020**, 95, 103497.
- [4] N. G. Kandile, H. T. Zaky, *J. Enzyme Inhib. Med. Chem.* **2015**, 30, 44.
- [5] T. H. Ibrahim, Y. M. Loksha, H. A. Elshihawy, D. M. Khodeer, M. M. Said, *Arch. Pharm. (Weinheim)* **2017**, 350, 1700093.
- [6] Z. Q. Dong, X. M. Liu, C. X. Wei, Z. S. Quan, *Med. Chem.* **2015**, 11, 595 <https://www.eurekaselect.com/article/65915>
- [7] B. Caliskan-Ergün, M. Süküroğlu, T. Coban, E. Banoğlu, S. Suzen, *J. Enzyme Inhib. Med. Chem.* **2008**, 23, 225.
- [8] T. Lüscher, J. Havelka, P. Greminger, J. Tuma, M. Tauber, W. Siegenthaler, W. Vetter, *Eur. J. Clin. Pharmacol.* **1982**, 23, 411.
- [9] M. Takaya, M. Sato, K. Terashima, H. Tanizawa, Y. Maki, *J. Med. Chem.* **1979**, 22, 53.
- [10] D. McTavish, E. M. Sorkin, *Drugs* **1989**, 38, 778.
- [11] E. N. Scott, G. Meinhardt, C. Jacques, D. Laurent, A. L. Thomas, *Expert Opin. Invest. Drugs* **2007**, 16, 367.
- [12] K. A. Manear, C. Adcock, R. Boulter, X. Cockcroft, L. Copey, A. Cranston, K. J. Dillon, J. Drzewiecki, S. Garman, S. Gomez, H. Javid, F. Kerrigan, C. Knights, A. Lau, V. M. Loh, I. T. W. Matthews Jr., S. Moore, M. J. O' Connor, G. C. M. Smith, N. M. B. Martin, *J. Med. Chem.* **2008**, 51, 6581.
- [13] Taniguchi, M., Hirose, M., Baba, M., Hirata, K., Ochiai, Y., Nissan Chemical Corp., 1983, US4877787A.
- [14] T. Jojima, Y. Takahi, *Ger. Offen.* **1977** DE 2640806.
- [15] T. Katayama, S. Kawamura, Y. Sanemistu, Y. Mine, *PCT Int. Appl.* **1997** WO 9707104.
- [16] B. R. Kim, S. D. Cho, H. G. Lee, H. S. Yim, M. J. Kim, J. Hwang, S. E. Park, J. J. Kim, K. J. Jung, Y. J. Yoon, *J. Heterocycl. Chem.* **2009**, 46, 691.

- [17] D. Asil, A. Cihaner, A. M. Önal, *Electrochim. Acta* **2009**, 54, 6740.
- [18] N. Atilgan, F. Algi, A. M. Önal, A. Cihaner, *Tetrahedron* **2009**, 65, 5776.
- [19] K. E. Ryu, B. R. Kim, G. H. Sung, H. J. Yoon, Y. J. Yoon, *Synlett* **1985**, 2015, 26.
- [20] H. K. Moon, G. H. Sung, B. R. Kim, J. K. Park, Y. J. Yoon, H. J. Yoon, *Adv. Synth. Catal.* **2016**, 358, 1725.
- [21] J. N. Lalpara, S. D. Hadiyal, A. J. Radia, J. M. Dhalani, G. G. Dubal, *Polycycl Aromat. Compd.* **2020**, 42(6), 3063.
- [22] J. N. Lalpara, M. D. Vachhani, S. D. Hadiyal, S. Goswami, G. G. Dubal, *Russ. J. Org. Chem.* **2021**, 57, 241.
- [23] S. D. Hadiyal, N. D. Parmar, P. L. Kalavadiya, J. N. Lalpara, H. S. Joshi, *Russ. J. Org. Chem.* **2020**, 56, 671.
- [24] A. J. Radia, J. N. Lalpara, I. J. Modasiya, G. G. Dubal, *J. Heterocycl. Chem.* **2021**, 58, 612.
- [25] S. D. Hadiyal, J. N. Lalpara, N. D. Parmar, H. S. Joshi, *Polycycl. Aromat. Compd.* **2021**, 42(7), 4752.
- [26] P. R. Vachharajani, M. J. Solanki, G. G. Dubal, V. H. Shah, *Pharma Chem.* **2011**, 3(1), 280.
- [27] M. D. Vachhani, J. N. Lalpara, S. D. Hadiyal, G. G. Dubal, *Russ. J. Org. Chem.* **2022**, 58, 356.
- [28] P. K. Talpara, G. G. Dubal, V. H. Shah, *Int. Lett. Chem. Phys. Astronom.* **2017**, 74, 9.
- [29] R. Monic, J. T. Gregory, H. D. Konstantin, R. R. James, *Cancer Treat. Rev.* **2013**, 39, 839.
- [30] A. O. Ademiluyi, G. Oboh, *Exp. Toxicol. Pathol.* **2013**, 65, 305.
- [31] L. J. Shai, P. Masoko, M. P. Mokgotho, S. R. Magano, A. M. Mogale, N. Boaduo, J. N. Eloff, *S. Afr. J. Bot.* **2010**, 76, 465.
- [32] R. R. Raju, A. M. Chari, K. Ravindar, M. C. T. Babu, W. Rajendra, D. Shobha, M. Ravichandar, K. Baburao, L. P. Swamy, *Eur. J. Med. Chem.* **2016**, 123, 379.
- [33] D. R. K. Patel, P. R. Tirgar, N. R. Jha, *J. Chem. Pharm. Res.* **2018**, 10, 41.
- [34] K. Pansuriya, J. N. Lalpara, S. D. Hadiyal, B. B. Dhaduk, G. G. Dubal, *Chem. Data Collect.* **2022**, 41, 100904.
- [35] K. K. Vukoti, S. P. Venkat, V. B. Ala, R. R. Radhakrishnam, K. R. S. Prasad, *Med. Chem. Res.* **2020**, 29, 528.

SUPPORTING INFORMATION

Additional supporting information can be found online in the Supporting Information section at the end of this article.

How to cite this article: A. J. Radia, J. N. Lalpara, S. D. Hadiyal, M. Kaneria, P. R. Tirgar, G. G. Dubal, *J. Heterocycl. Chem.* **2022**, 1. <https://doi.org/10.1002/jhet.4615>